AFRL-RQ-WP-TP-2015-0046

STRUCTURAL RESPONSE PREDICTION: FULL-FIELD, DYNAMIC PRESSURE AND DISPLACEMENT MEASUREMENTS OF A PANEL EXCITED BY SHOCK BOUNDARY-LAYER INTERACTION

S. Michael Spottswood, Timothy J. Beberniss, and Thomas G. Eason

Hypersonic Sciences Branch
High Speed Systems Division

FEBRUARY 2015
Interim Report

AIR FORCE RESEARCH LABORATORY
AEROSPACE SYSTEMS DIRECTORATE
WRIGHT-PATTERSON AIR FORCE BASE, OH 45433-7541
AIR FORCE MATERIEL COMMAND
UNITED STATES AIR FORCE

NOTICE AND SIGNATURE PAGE

Using Government drawings, specifications, or other data included in this document for any purpose other than Government procurement does not in any way obligate the U.S. Government. The fact that the Government formulated or supplied the drawings, specifications, or other data does not license the holder or any other person or corporation; or convey any rights or permission to manufacture, use, or sell any patented invention that may relate to them.

This report was cleared for public release by the USAF 88th Air Base Wing (88 ABW) Public Affairs Office (PAO) and is available to the general public, including foreign nationals.

Copies may be obtained from the Defense Technical Information Center (DTIC) (http://www.dtic.mil).

AFRL-RQ-WP-TP-2015-0046 HAS BEEN REVIEWED AND IS APPROVED FOR PUBLICATION IN ACCORDANCE WITH ASSIGNED DISTRIBUTION STATEMENT.

*//Signature//
S. MICHAEL SPOTTSWOOD
Program Manager
Hypersonic Sciences Branch
High Speed Systems Division

//Signature//
MEI-LING LIBER, Branch Chief
Hypersonic Sciences Branch
High Speed Systems Division

//Signature//
PATRICIA D. PEARCE, Deputy Division Chief
High Speed Systems Division
Aerospace Systems Directorate

This report is published in the interest of scientific and technical information exchange, and its publication does not constitute the Government's approval or disapproval of its ideas or findings.

*Disseminated copies will show "//Signature//" stamped or typed above the signature blocks.

REPORT DOCUMENTATION PAGE

Form Approved
OMB No. 0704-0188

1. REPORT DATE *(DD-MM-YY)*	2. REPORT TYPE	3. DATES COVERED *(From - To)*
February 2015	Interim	01 October 2011 – 30 September 2013

4. TITLE AND SUBTITLE
STRUCTURAL RESPONSE PREDICTION: FULL-FIELD, DYNAMIC PRESSURE AND DISPLACEMENT MEASUREMENTS OF A PANEL EXCITED BY SHOCK BOUNDARY-LAYER INTERACTION

5a. CONTRACT NUMBER
In-house

5b. GRANT NUMBER

5c. PROGRAM ELEMENT NUMBER
61102F

6. AUTHOR(S)
S. Michael Spottswood, Timothy J. Beberniss, and Thomas G. Eason (AFRL/RQHF)

5d. PROJECT NUMBER
3002

5e. TASK NUMBER
N/A

5f. WORK UNIT NUMBER
Q185

7. PERFORMING ORGANIZATION NAME(S) AND ADDRESS(ES)
Hypersonic Sciences Branch (AFRL/RQHF)
High Speed Systems Division
Air Force Research Laboratory, Aerospace Systems Directorate
Wright-Patterson Air Force Base, OH 45433-7541
Air Force Materiel Command, United States Air Force

8. PERFORMING ORGANIZATION REPORT NUMBER
AFRL-RQ-WP-TP-2015-0046

9. SPONSORING/MONITORING AGENCY NAME(S) AND ADDRESS(ES)
Air Force Research Laboratory
Aerospace Systems Directorate
Wright-Patterson Air Force Base, OH 45433-7541
Air Force Materiel Command
United States Air Force

10. SPONSORING/MONITORING AGENCY ACRONYM(S)
AFRL/RQHF

11. SPONSORING/MONITORING AGENCY REPORT NUMBER(S)
AFRL-RQ-WP-TP-2015-0046

12. DISTRIBUTION/AVAILABILITY STATEMENT
Approved for public release; distribution unlimited.

13. SUPPLEMENTARY NOTES
PA Case Number: 88ABW-2015-0385; Clearance Date: 02 Feb 2015.

14. ABSTRACT
The United States Air Force has attempted to field a hypersonic vehicle for decades. Time and time again, experimental vehicle programs have been initiated only to have been prematurely canceled. Although the reasons for early program termination are many, some interesting structural concerns have promulgated the history of these hypersonic vehicle efforts. Hypersonic vehicle design occurs at the intersection of aero-thermal-elastic disciplines, and to design, analyze and field a production-quality vehicle will require an appreciation and consideration of those intersecting disciplines. One specific area of concern has been the effect of shock boundary-layer interaction (SBLI) on the local response of outer mold line (OML) vehicle panel-structure. Vehicle bow-shocks and shocks emanating from vehicle corners, protuberances, compression ramps and control surfaces can lead to an amplification of temperature and fluctuating pressures or even couple with structural modes of vibration in turn leading to premature and unanticipated structural failures. To that end, a series of experiments have been started to investigate the response of a compliant aircraft-like panel to turbulent boundary layer noise and shock interactions. Specifically, the purpose of the present experimental investigation is twofold: 1) to develop the necessary full-field, non-contacting measurement techniques that allow for complete characterization of the structural loading and response, and 2) to gauge the impact of SBLI on the response of the structure. This work, as opposed to other studies, focuses on the low-frequency content in the turbulent boundary layer that is prone to couple with the structure. This low-frequency emphasis necessitates long data time-records. Full-field fast-reacting pressure sensitive paint (PSP) and non-contact optical displacement results are presented detailing the effect of the turbulent and SBLI flow conditions on the structure. The full-field experimental data was reduced using dynamic and proper orthogonal modes for the surface pressures and operational modal analysis for the corresponding dominant structural deflected shapes. The modes and spectral results, along with observations regarding spatial surface pressure averaging, are presented and discussed.

15. SUBJECT TERMS

16. SECURITY CLASSIFICATION OF:			17. LIMITATION OF ABSTRACT:	18. NUMBER OF PAGES	19a. NAME OF RESPONSIBLE PERSON (Monitor)
a. REPORT	b. ABSTRACT	c. THIS PAGE			S. Michael Spottswood
Unclassified	Unclassified	Unclassified	SAR	24	19b. TELEPHONE NUMBER *(Include Area Code)* N/A

Structural Response Prediction: Full-field, dynamic pressure and displacement measurements of a panel excited by shock boundary-layer interaction

S. Michael Spottswood[1], Timothy J. Beberniss[2], Thomas G. Eason[1]
Air Force Research Laboratory, Wright-Patterson AFB, Ohio, 45433

The United States Air Force has attempted to field a hypersonic vehicle for decades. Time and again experimental vehicle programs have been initiated only to have been prematurely canceled. Although the reasons for early program termination are many, some interesting structural concerns have promulgated the history of these hypersonic vehicle efforts. Hypersonic vehicle design occurs at the intersection of aero-thermal-elastic disciplines, and to design, analyze and field a production-quality vehicle will require an appreciation and consideration of those intersecting disciplines. One specific area of concern has been the effect of shock boundary-layer interaction (SBLI) on the local response of outer mold line (OML) vehicle panel-structure. Vehicle bow-shocks and shocks emanating from vehicle corners, protuberances, compression ramps and control surfaces can lead to an amplification of temperature and fluctuating pressures or even couple with structural modes of vibration in turn leading to premature and unanticipated structural failures. To that end, a series of experiments have been started to investigate the response of a compliant aircraft-like panel to turbulent boundary layer noise and shock interactions. Specifically, the purpose of the present experimental investigation is twofold: (1) to develop the necessary full-field, non-contacting measurement techniques that allow for complete characterization of the structural loading and response, and (2) to gauge the impact of shock boundary layer interaction on the response of the structure. This work, as opposed to other studies, focuses on the low-frequency content in the turbulent boundary layer that is prone to couple with the structure. This low-frequency emphasis necessitates long data time-records. Full-field fast-reacting pressure sensitive paint (PSP) and non-contact optical displacement results are presented detailing the effect of the turbulent and Shock Boundary-Layer Interaction (SBLI) flow conditions on the structure. The full-field experimental data was reduced using dynamic and proper orthogonal modes for the surface pressures and operational modal analysis for the corresponding dominant structural deflected shapes. The modes and spectral results, along with observations regarding spatial surface pressure averaging, are presented and discussed.

I. Introduction

The Air Force Research Lab (AFRL) Structural Sciences Center (SSC) at Wright-Patterson Air Force Base, Ohio, is focused on furthering the understanding and developing the necessary framework to simulate the evolution of extreme-environment structures throughout a hypersonic trajectory. This simulation perspective is necessary to capture the path-dependent environment (structural driving forces) and corresponding structural response in lieu of the traditional aircraft design perspective of superposing the worst possible loading scenarios and conditions in an attempt to produce the most conservative design[1,2]. Hypersonic, extreme-environment air vehicles require structures that can withstand intense complex loading scenarios. These structural designs will experience extremely high, transient surface temperatures and thermal gradients from flow compression and viscous dissipation, significant dynamic pressure fluctuations due to boundary layer turbulence, engine noise, deformation induced pressures, and long-duration exposure to these environments[3,4]. Challenges in predicting the response of surface panels on hypersonic vehicles include: (1) the coupling between thermal-fluid-structural response; (2) the identification and modeling of local effects inherent in hypersonic flows; (3) material nonlinearity, temperature dependence and

[1]Senior Aerospace Research Engineer, Aerospace Systems Directorate/RQHF, 2790 D Street, Non-Member.
[2]Aerospace Research Engineer, Aerospace Systems Directorate/RQHF, 2790 D Street, Non-Member.

degradation; (4) the spatial variation of material and structural properties; and (5) the uncertainty in loads, material properties, and geometry and boundary conditions. Compounding these analysis and design challenges are the failure modes of high-speed vehicle structures. These structures can fail in high-cycle fatigue due to severe aero-acoustic and mechanical vibration loading, in low-cycle fatigue due to thermal-mechanical loading, and by material degradation due to the extreme thermal environment[5].

The design of efficient structures for hypersonic vehicles requires structural analysts and designers to accurately characterize the environment, and in particular, the aero-acoustic and engine-induced dynamic environment. Maestrello and Linden[6] as well as Coe and Chyu[7] both studied the effects of high-speed flow, including shock boundary-layer interaction, on panel structures. Maestrello noted that impinging shock waves result in severe dynamic loading with the potential for shock oscillations to couple with the air vehicle panel vibratory modes. Coe and Chyu conducted an extensive series of experiments to characterize the dynamic pressure fluctuations for attached and separated flow, and for shock boundary-layer interaction conditions at various Mach numbers. Results of their seminal work have been used to derive aero-acoustic empirical and semi-empirical prediction methods. Pozefsky[8] predicted sonic/acoustic-fatigue prone critical regions on a hypersonic Transatmospheric Vehicle (TAV) noting that the proposed vehicle will experience severe acoustic environments with local flow separation and shock impingement amplifying the expected fluctuating pressures resulting in large out-of-plane deformations (geometric nonlinearity). Dolling[9,10] notes that shock-wave boundary-layer interaction can have severe impact on high-speed aircraft structures, and further, notes the limitations on predicting that fluctuating pressure environment.

The purpose of this on-going experiment is to investigate the response of an aircraft-like panel in the presence of an impinging, oblique shock-wave and to characterize the resulting full-field pressure and displacement relationships[11-13]. The goals of this experimental program include: (1) a measure of the turbulent boundary layer and shock impingement/oscillation effects on a compliant panel; (2) a measure of the flow-induced pressure correlation across the panel; (3) the impact of panel vibrations on the near-field fluctuating pressure characteristics; and (4) to explore, and extend where necessary, full-field measurement techniques in order to capture the dynamic loading and nonlinear response of a flexible panel in this high-speed flow environment.

II. Experimental Configuration

The current series of experiments are being conducted in the AFRL Aerospace Systems Directorate large-scale RC-19 supersonic combustion research cell[14]. The RC-19 facility is a continuous flow wind tunnel designed to study the mechanisms that govern the mixing and combustion process for supersonic combustor geometries. The RC-19 research facility was modified two years ago to accommodate the present aerothermoelastic experiment. A sectional view of the tunnel arrangement is shown in Figure 1. All testing was conducted at Mach 2.0, free-stream dynamic pressures (q_∞) of 61.7, 91.4, and 123 kPa, and total pressures of 172, 255, and 345 kPa. Free-stream and stagnation conditions are referenced to the tunnel nozzle exit. The Mach 2 nozzle is located upstream of the test section, while the test section consists of four separate interchangeable walls that can be configured to meet a variety of experimental requirements. For this study, a 305 mm x 152 mm x 12.7 mm block of ANSI 4150 alloy steel was machined to create the compliant panel. A pocket was machined into the block leaving 0.635 mm for the compliant panel thickness over an effective vibration dimension of 254 mm long by 127 mm wide. A rigid, control specimen without a machined pocket was also manufactured. The flexible panel specimen was designed so that an appreciable number of the structural dynamic modes would be below 1000 Hz. The tunnel test-section top-wall was redesigned to accept the compliant panel, and a series of pressure ports were made available for static and dynamic pressure measurements upstream of the panel. Additionally, pressure ports were added to the top section of the

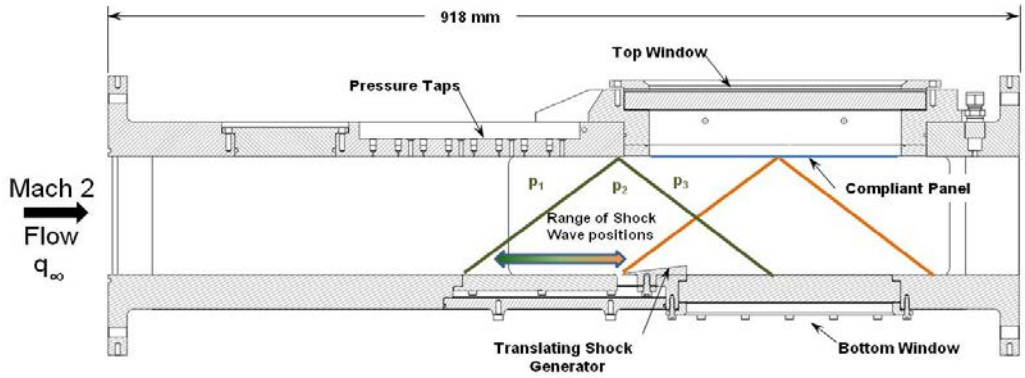

Figure 1: RC-19 Tunnel Test-Section

tunnel wall downstream of the compliant panel to equalize the pressure between the panel and the top window. This window was used to allow image acquisition using Digital Image Correlation (DIC) to obtain the full field displacements. Equalization of the pressure was necessary to prevent yielding of the panel during tunnel start-up. The sides of the tunnel contained large windows to allow for PSP illumination and implementation of a shadowgraph set-up to visualize the flow. A window was also added to the bottom wall test section to allow for viewing the PSP on the flow-side of the compliant panel. When the shock generator was used, it was placed in the bottom wall of the tunnel turning the flow 8° resulting in a shock wave angle of 39° from the tunnel bottom wall. The shock generator can translate 170 mm in the flow direction to allow for the shock wave to impinge from the compliant panel leading edge to nearly the half-point as shown in Figure 1. The boundary layer thickness without the shock generator is 7.6 mm where the flow first meets the panel and grows to 10.2 mm at the end of the panel[14].

The top of the panel specimen was prepared for DIC by first uniformly painting the specimen using a standard flat-white paint followed by a hand-applied random pattern of flat-black dots using a permanent, fine-tipped marker. The randomness of the pattern is crucial to avoid spatial aliasing of the digital images which can then lead to displacement measurement bias[15]. The dot pattern was applied to the entire top-surface of the specimen and to one area of the specimen frame so that panel relative displacement measurements could be made. This process was previously demonstrated to provide the greatest displacement range during random, dynamic testing[11]. Further, applying the DIC pattern across the entire top-surface provided the flexibility to interrogate any desired panel location post-test. For all DIC data acquisition the following analysis software, calibration, cameras, and settings were used. The DIC software used in this study was the GOM Optical Measuring Technique's IVIEW Real-Time Sensor for dynamic analysis and ARAMIS for static analysis. Through a collaborative effort between AFRL and GOM the IVIEW program was modified to accommodate the large volumes of images required for random-vibration measurement. The calibration object used was a GOM specific 250 x 200 mm panel with a 150.01 mm calibration scale. The two cameras used in the testing were Photron SA5's with 32 GB of memory and 28 mm lenses set at an aperture of 2.8. The resulting camera calibration produced a measurement volume of 425 x 450 x 450 mm. The calibration deviation was 0.021 pixels and the reported camera angle was 25.8 degrees. The camera resolution for specimen measurement was 768 x 496 pixels and the frame rate was 4000 frames per second (fps). Specimen illumination consisted of a 305 x 305 mm Litepanel which is a panel array of 1152 LED bulbs for a consistent distribution of lighting that also minimizes specimen heating and therefore pre-stress. Two banner white high intensity area lights model LEDRA70D4-XQ were also used to help alleviate shadows caused by the cavity walls. A total of 22.5 seconds at a sampling rate of 4 kHz was recorded using this arrangement.

The bottom or flow-side of the rigid (control) and flexible panel specimens were painted with the fast-response binary FIB PSP paint from Innovative Scientific Solutions Inc[16,17] applied on the day of testing. In order to accomplish this, it was necessary to remove the panel specimen from the tunnel due to the confined area within the tunnel. After drying, the panel specimen was reinstalled and a structural modal test was performed on the panel to ensure proper installation. Illumination for the PSP was provided by two LM2X-400 LED heads entering through the side windows and triggered "on" 5 seconds prior to image acquisition and turned off after the acquisition of all images was completed. During testing, the change in paint luminescence was related to the partial pressure of oxygen and calibrated to a known reference pressure. The return light from the panel exited through a window in the bottom of the tunnel and was reflected by a mirror to the PSP camera. The camera, also a Photron SA5 with 32 GB of memory, was used to record the full-field PSP pressure measurements (14.5 seconds sampled at 4 kHz) triggered simultaneously with the DIC measurements. The PSP field of view was 195 mm in the flow direction and

155 mm in the transverse direction with the each pixel representing a physical sensor size of 0.278 mm by 0.278 mm. The images were cropped in the transverse direction to match the physical plate width.

The experimental procedure began by pulling a vacuum on the tunnel to an approximate absolute pressure of 20.5 kPa. A series of "wind-off" images for PSP were collected at that time. The tunnel was then started by setting the total pressure at the nozzle to the desired value. Before starting the tunnel, the test section was at room temperature so the compliant panel frame, which is not exposed to the flow, required an initial waiting period to achieve temperature equilibrium between the compliant panel and the frame. The temperature difference between the panel and frame induced a transient thermal stress that decayed over time altering the dynamic response of the panel. Laser vibrometry was used to probe the dynamic response of the compliant panel until the dynamic response showed little difference in the power-spectral density (PSD) response over a five minute period. At this point, the cameras used for the 3D DIC and PSP (wind-on images) were triggered at the same time and images recorded for approximately 22.5 seconds at a 4 kHz rate for the DIC and 14.5 seconds at 4 kHz for the PSP images. One consequence of these long-time records (required for spectral analysis and averaging purposes) was the tremendous amount of data (camera images) generated for each RC-19 wind tunnel test run. Simultaneous laser vibrometry data and strain gage data were recorded on a separate data acquisition system for 60 seconds of time at a sampling rate of 20 kHz. Additionally, two more data acquisition systems were employed. One was used to gather static data while the other was dedicated to the fluctuating pressure measurements. The images were then downloaded from the camera memory using separate computers for each of the three cameras to decrease download time to approximately 30 minutes. This process was repeated for each test run. The crowded RC-19 test section and associated testing equipment is shown in Figure 2.

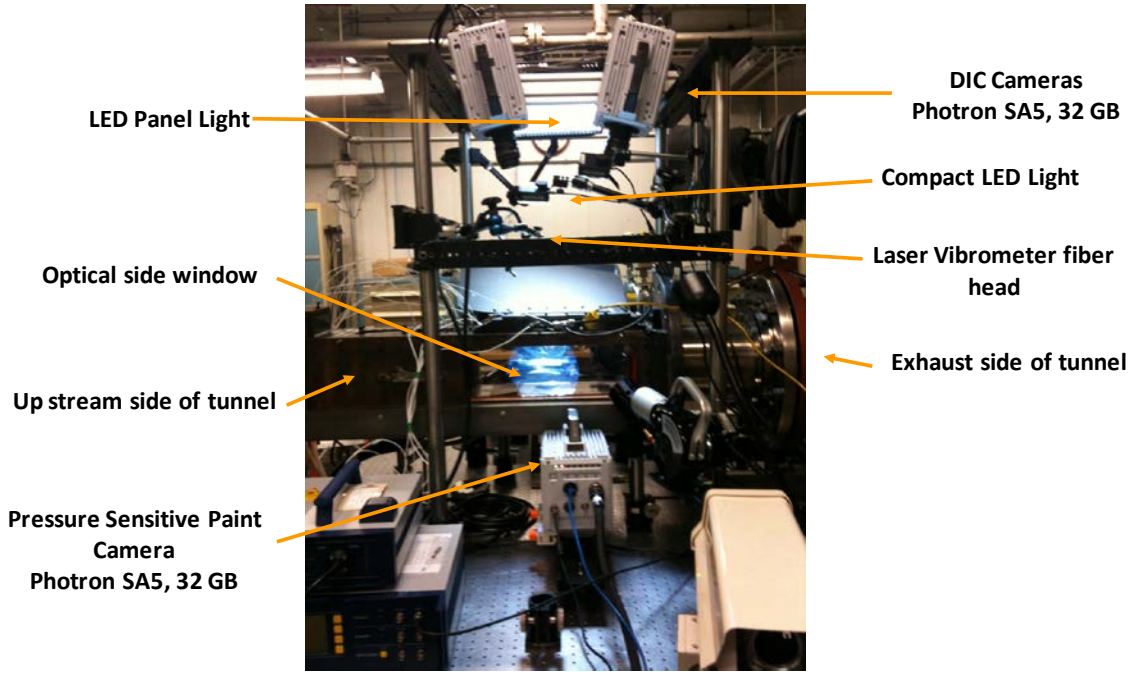

Figure 2: RC-19 Test-Section with Digital Image Correlation (DIC) and Pressure Sensitive Paint (PSP) test configuration.

In the present study a 153-point 20x20-averaged pixel facet array was developed to survey the response across the panel and provide sufficient measurement locations for operational modal analysis (OMA) based panel deformation identification. For reference a DIC facet is an area of selected pixels over which the panel response is averaged in turn reducing system noise[18]. The additional patterned area on the specimen frame was used to obtain the relative response of the panel with respect to unwanted but unavoidable tunnel vibration. The panel with the applied DIC pattern, 153-facet DIC array, and single measurement location on the frame is shown in Figure 3.

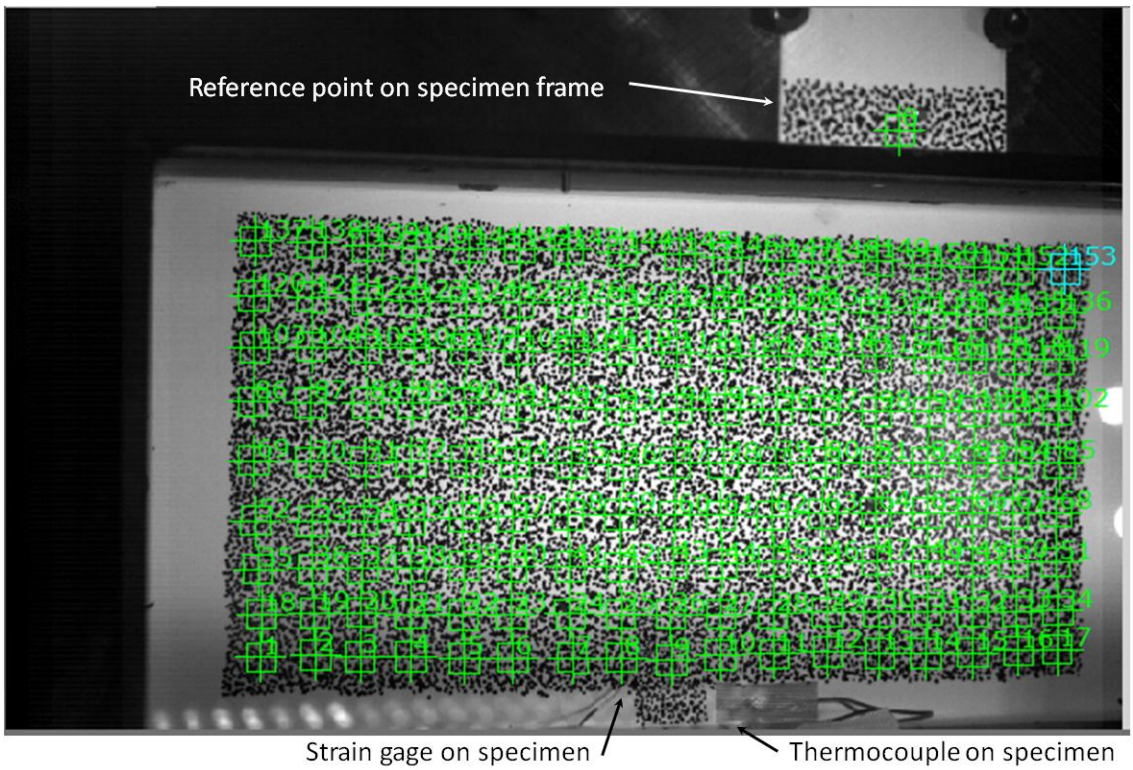

Figure 3: Specimen panel top-surface and frame with applied DIC pattern, and superposed array of displacement measurement locations.

III. Preliminary Results & Discussion

The principal purpose of the experiment was to ascertain the effects of the turbulent boundary layer and shock impingement on the response of the panel specimen while simultaneously recording the full-field surface pressure and panel dynamic displacement. One test condition considered in the present study had the shock generator positioned such that the primary oblique shock impinged on the panel at approximately 1/3 of the panel length downstream of leading edge. This particular shock generator position resulted in the most significant panel dynamic response with panel center displacement and strain standard deviations of 0.089 mm and 78 με respectively, and peak displacements of 0.36 mm (57% of the panel thickness). The average strain for this experimental flow case was 627 με, with excursions to 968 με. The results of this particular test condition and the test condition repeated with heated flow are shown in Figure 4. The effect of the tunnel differential pressure during the test run is noticeable when observing the stiffening effect on the panel vibration modes. Note that the abscissa includes marks for the frequencies of the unstressed panel vibration modes. These modes, along with accompanying viscous damping values, were measured before testing using a single degree of freedom (SDOF) Rational Fraction Polynomial (RFP) frequency domain modal analysis technique[19]. The techniques are quite straightforward. First the frequency response function (FRF) was estimated from the experimental input and output measurements, where the FRF is defined as the following transfer function:

$$H_{pq}(\omega) = \frac{\sum_{k=0}^{n} \beta_k (j\omega)^k}{\sum_{k=0}^{m} \alpha_k (j\omega)^k} \tag{1}$$

Next the unknown coefficients, α_k and β_k, can be solved for in a least-squares sense when the expression is rearranged into the following convenient form:

$$[\alpha_0\alpha_1 \cdots \alpha_m\beta_0\beta_1 \cdots \beta_n]\begin{bmatrix}(j\omega)^0 H_{pq}(\omega)\\(j\omega)^1 H_{pq}(\omega)\\\vdots\\(j\omega)^m H_{pq}(\omega)\\-(j\omega)^0\\-(j\omega)^1\\\vdots\\-(j\omega)^n\end{bmatrix} = 0 \tag{2}$$

The identified scalar coefficients, α_k, are next used in the assembly of a companion matrix:

$$\boldsymbol{C} = \begin{bmatrix}-\alpha_{m-1} & -\alpha_{m-2} & \cdots & -\alpha_1 & -\alpha_0\\1 & 0 & \cdots & 0 & 0\\0 & 1 & \cdots & 0 & 0\\0 & 0 & \cdots & 0 & 0\\\vdots & \vdots & \ddots & \vdots & \vdots\\0 & 0 & \cdots & 0 & 0\\0 & 0 & \cdots & 0 & 0\\0 & 0 & \cdots & 1 & 0\end{bmatrix} \tag{3}$$

The eigenvalue decomposition of the companion matrix provides the system frequencies and damping, and possibly the mode shapes in the case of the multiple-input, multiple output RFP approach. In the case of a frequency domain approach, the complex eigenvalues (poles) of the companion matrix, $\lambda_r = \sigma_r + j\omega_r$, consist of the modal damping, σ_r, and the damped natural frequency, ω_r, for the r^{th} mode. For time domain modal analysis, the eigenvalues of the companion matrix must be logarithmically mapped to the complex domain. The first six measured system frequencies and damping values using this approach are listed in Table 1. Modal testing was done both before and after testing this specimen in the wind tunnel to quantify any changes to the panel, and there were no substantive changes.

	Frequency (Hz)		Damping Ratio (%)	
Mode	Pretest	Post	Pretest	Post
(1,1)	208	209	0.16	0.22
(2,1)	225	225	0.14	0.21
(3,1)	334	335	0.07	0.13
(4,1)	499	499	0.06	0.11
(1,2)	565	563	0.07	0.11
(2,2)	612	608	0.06	0.09

Table 1: Test panel pre- and post-test measured frequencies and damping.

In the dynamic response of Figure 4, clearly the first panel mode dominates the response for both the heated and unheated case. The deflected shapes displayed in Figure 3 are the result of applying output-only modal analysis to the full-field displacement (output) results using the DIC measurements versus the traditional modal analysis procedure just described[20]. The presented deflected shapes are the singular vectors resulting from the decomposition of the Hermitian auto- and cross-spectral density matrix. The DIC measurement points are first transformed into the frequency domain via the Fast Fourier Transform (FFT). The FFT spectral estimation was processed using a blocksize of 2048 data points and a Hanning window with 50% overlap. Next, the auto- and cross-spectral density matrix was populated at the resulting discrete frequencies as follows:

$$\boldsymbol{G_{yy}} = \begin{bmatrix}\boldsymbol{G_{11}}(\omega) & \boldsymbol{G_{12}}(\omega) & \cdots & \boldsymbol{G_{1n}}(\omega)\\\boldsymbol{G_{21}}(\omega) & \boldsymbol{G_{22}}(\omega) & & \\\vdots & & \ddots & \\\boldsymbol{G_{n1}}(\omega) & & & \boldsymbol{G_{nn}}(\omega)\end{bmatrix} \tag{4}$$

where $\boldsymbol{G_{yy}}$ is the ensemble-averaged output DIC spectral density matrix, the main diagonal terms are the auto-spectral densities while the off-diagonal terms are the cross-spectral densities of the output DIC measurement points. The spectral density matrix is Hermitian so $\boldsymbol{G_{pq}(\omega)} = \boldsymbol{G_{qp}}^{*}\boldsymbol{(\omega)}$ for $p \neq q$, where the asterisk denotes the complex conjugate. Finally, the spectral density matrix is decomposed at each i^{th} frequency using singular value decomposition (SVD):

$$\boldsymbol{G_{yy}}(\omega_i) = \boldsymbol{\Phi_i \Sigma_i \Phi_i^H} \tag{5}$$

where $\boldsymbol{\Phi_i}$ is a unitary matrix of singular vectors, $\boldsymbol{\Phi_i = [\Phi_1, \Phi_2, ..., \Phi_n]}$, and $\boldsymbol{\Sigma_i}$ is the corresponding matrix of singular values. The singular vectors resulting from the decomposition of the power spectral density matrix approximate the system mode shapes for a lightly-damped system under broadband-excitation. This approach is similar to the Complex Mode Indicator Function (CMIF), where the FRF matrix is decomposed at each frequency using singular value decomposition[21]. The relative magnitude of the singular values at each frequency denotes the relative modal contribution. Each of the operational deflected shapes in Figure 4 corresponds to the maximum singular value for that particular frequency. An obvious benefit of the full-field DIC displacement response is the ability to interrogate a number of points sufficient to describe the deflected shapes as a function of frequency. Note the deformation bias in the panel deflected shapes resulting from the asymmetric shock impingement with the generator in position 1. Note also the frequencies of the unstressed panel modes denoted on the frequency axis and as vertical lines. For this test case, the Mode (1,1) frequency increased approximately 90-Hz. As mentioned, the flexible panel specimen was designed so that an appreciable number of dynamic modes would be excited below 1000-Hz, typical of aircraft structures.

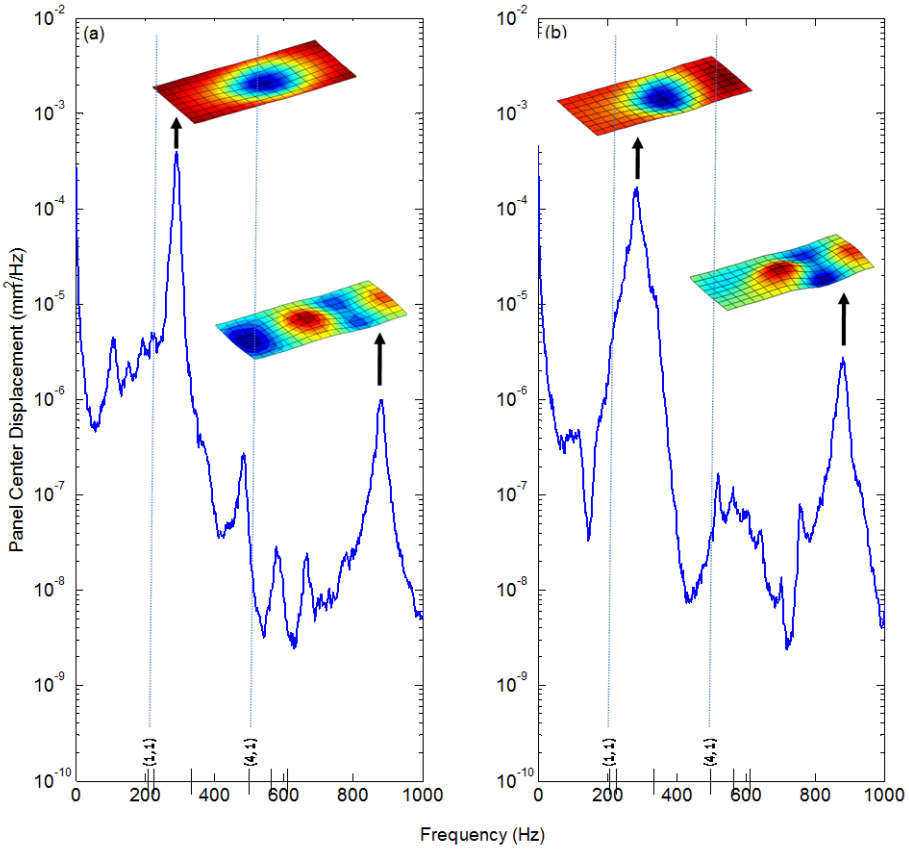

Figure 4: Panel displacement PSD and accompanying deflected shapes (M_∞ = 2.0, q_∞ = 123-kPa) for the (a) unheated and (b) heated flow conditions.

Figure 5 shows the corresponding averaged (in space) PSP results for the same flow condition represented in Figure 4. A 9 by 9-pixel moving spatial average was used for each PSP image recorded during testing. In addition to the full PSP image of Figure 5, the reduced-size box-section and single point represent the surface area and single-pixel considered in the subsequent analyses.

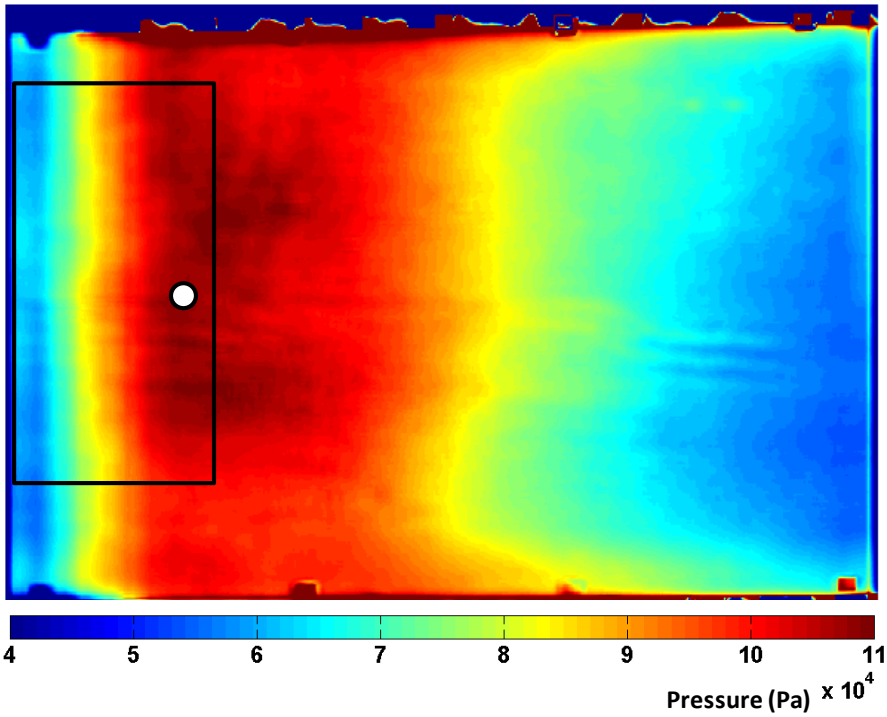

Figure 5: Spatially averaged PSP (M_∞ = 2.0, q_∞ = 123-kPa).

Just like the DIC results, the full-field, high-frequency PSP afforded the opportunity to investigate the compliant panel surface pressure "modes" using both proper orthogonal and dynamic mode analysis[22,23,24,25]. Dynamic mode decomposition (DMD) is a time-domain, nonparametric identification method used to extract the dynamic characteristics (eigenvalues/vectors) from a series of full-field numerical or experimental data snap-shots equally spaced in time. One difference between the RFP modal analysis method previously described and DMD is that DMD does not assume a model form. The data (experimental in this case) is first assembled in the following column-vector format with notation following that of Schmid[25]:

$$\boldsymbol{V_1^{N-1}} = \{\boldsymbol{v_1}, \boldsymbol{v_2}, \cdots, \boldsymbol{v_{N-1}}\} \tag{6}$$

Each column vector represents the spatial information at a discrete and equally-spaced time step. The assumptions of the method are that (1) the snapshot data at time-step N can be described by a linear combination of previous snapshots (causal):

$$\boldsymbol{V_2^N} = \boldsymbol{A}\boldsymbol{V_1^{N-1}} \tag{7}$$

where $\boldsymbol{A}$ is a linear mapping between $\boldsymbol{V_2^N}$ and $\boldsymbol{V_1^{N-1}}$. The DMD process seeks to characterize the dynamics described by this linear mapping. Assumption (2) is that there are sufficient snapshots such that the retained vectors span the data-space. When assumption (2) is realized, the dataset array $\boldsymbol{v_N}$ is formulated as a linear combination of the previous, linearly independent vectors:

$$\boldsymbol{v_N} = a_1\boldsymbol{v_1} + a_2\boldsymbol{v_2} + \cdots + a_{N-1}\boldsymbol{v_{N-1}} + \boldsymbol{r} = \boldsymbol{V_1^{N-1}}\boldsymbol{a} + \boldsymbol{r} \tag{8}$$

where $\boldsymbol{r}$ is the residual vector and a_i the scalar coefficients that represent the linear relationship between the snapshot vectors. The set of vectors $\boldsymbol{V_2^N}$ can now be written as:

$$\boldsymbol{V_2^N} = \{\boldsymbol{v_2}, \boldsymbol{v_3}, \cdots, \boldsymbol{V_1^{N-1}a}\} + \boldsymbol{re_{N-1}^T} = \boldsymbol{V_1^{N-1}S} + \boldsymbol{re_{N-1}^T} \tag{9}$$

where $\boldsymbol{e_{N-1}^T}$ is the $\boldsymbol{(N\text{-}1)^{th}}$ unit vector and $\boldsymbol{S}$, similar to the experimental RFP modal analysis procedure described previously, is of a companion matrix form, *i.e.*, both methods share the same characteristic polynomial form:

$$\boldsymbol{S} = \begin{bmatrix} 0 & 0 & \cdots & 0 & a_1 \\ 1 & 0 & & 0 & a_2 \\ 0 & 1 & & 0 & a_3 \\ \vdots & & \ddots & & \vdots \\ 0 & 0 & \cdots & 1 & a_{N-1} \end{bmatrix} \tag{10}$$

Finally, the eigenvectors, or dynamic modes, of the linear mapping matrix are realized, by definition, as the eigenvectors of the companion matrix pre-multiplied by the snapshot vectors, $\boldsymbol{V_1^{N-1}}$. The eigenvalues of the companion matrix, also the eigenvalues of the linear mapping matrix, are mapped to the complex domain resulting in the system frequencies and damping. This approach, while applied relatively recently in the fluids-community, is common to analyses in other disciplines and is in fact equivalent to the forward auto-regressive modeling approach for linear systems analysis, itself a subset of the autoregressive moving average (ARMA) model.

In addition to the DMD analysis, the proper orthogonal modes (POM) of the surface pressure results were also estimated. Proper orthogonal decomposition, or principal component analysis, Karhunen–Loève transform, etc., is used to identify coherent structures in a series of data snapshots. These coherent structures can be used in reduced order modeling where for instance the dynamical system is projected onto a truncated, compact set of retained modes. These modes are calculated as follows[26]. First, a surface pressure correlation matrix is formed:

$$\boldsymbol{R} = \tfrac{1}{N}(\boldsymbol{V^N})(\boldsymbol{V^N})^{\boldsymbol{T}} \tag{11}$$

where the columns of $\boldsymbol{V^N}$ are the spatial coordinates while the rows represent the time components. The POMs are next calculated from an Eigen-analysis of the correlation matrix:

$$\boldsymbol{R\Psi} = \varphi\boldsymbol{\Psi} \tag{12}$$

with POMs $\boldsymbol{\Psi} = [\boldsymbol{\Psi_1}, \boldsymbol{\Psi_2}, ..., \boldsymbol{\Psi_n}]$. Equivalently, the left singular vectors of the data snapshot matrix $\boldsymbol{V^N}$ also contain the proper orthogonal modes[24]. Both the DMD and POM methods were used in the analysis of the surface pressure data in an initial attempt to characterize the overall surface-pressure conditions. A benefit of the DMD analysis is that the resulting modes have an associated frequency and damping and can therefore be related to the surface displacement dynamics.

Figure 6 displays the time history and PSD for the single point denoted in Figure 5. Also displayed is the dynamic mode (DMD) for the full image calculated at the spectral peak of 290 Hz. Note that this frequency corresponds to the first panel mode displayed in Figure 4. Other than the leading edge periodicity, the dynamic mode in this case displays some interesting striations the authors believe may be a function of the applied PSP. Also displayed in Figure 6 are the normalized magnitudes for several key dynamic modes again from the full-panel snapshot analysis. One interesting observation is the very low frequency oscillations (~9 Hz) in the time history and frequency domain of Figure 6.

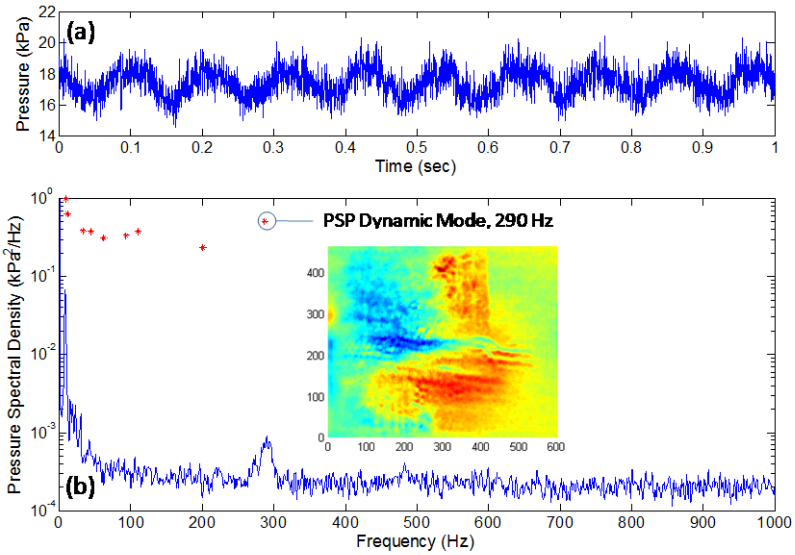

Figure 6: (a) PSP time history, and (b) PSD with corresponding dynamic modes.

Next, a smaller region of the full-PSP image was considered for the DMD analysis. This smaller region is the "box" region noted in Figure 5 and away from the possible inconsistencies in the applied PSP. Figure 7 and Figure 8 display the first eight proper orthogonal and dynamic modes corresponding to this region respectively.

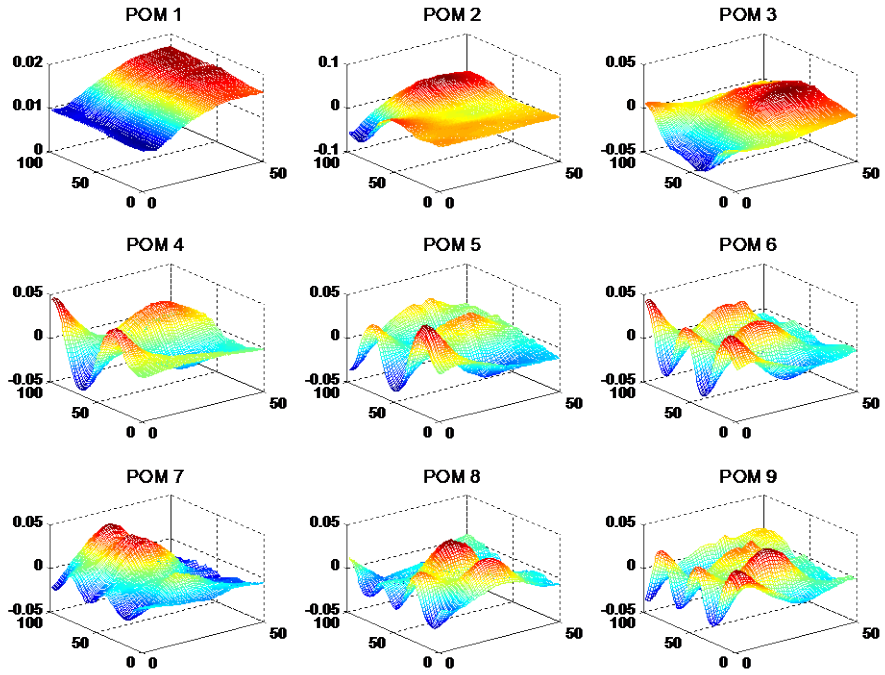

Figure 7: First 9 PSP proper orthogonal modes (POMs).

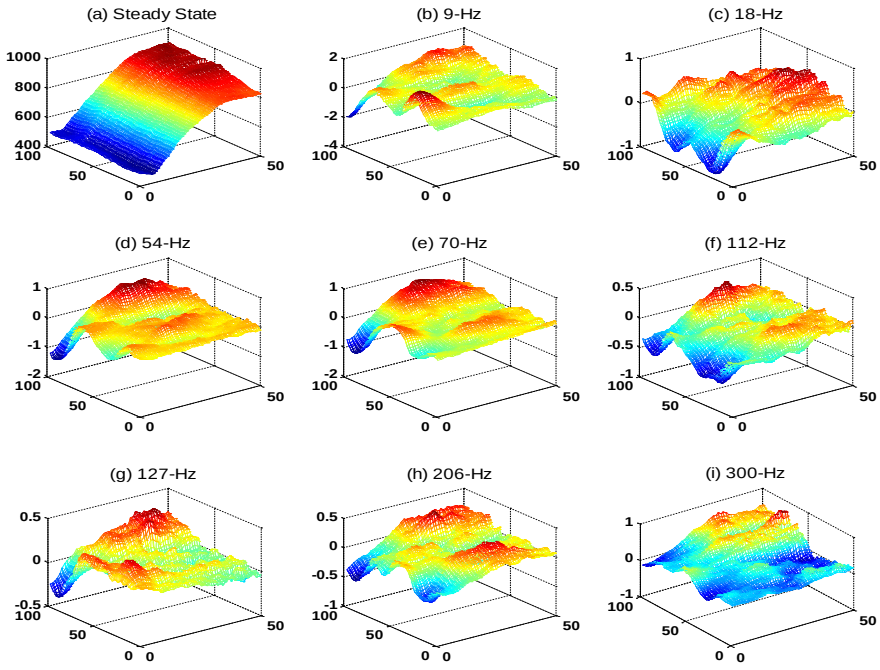

Figure 8: Dominant PSP dynamic modes.

One issue with using the dynamic modes to characterize the present surface pressure results was the preponderance of low-frequency content from the wind tunnel. In fact, the low frequency tunnel dynamic modes dominated the results, with the exception of the 300 Hz mode. To investigate the tunnel noise issue, consider the tunnel and test-article spectral content of Figure 9. The PSP and DIC measurements on the compliant panel are from the center of the panel. Additional DIC results are shown for the reference point on the frame as shown in Figure 9 as well as the transverse tunnel displacement up-stream of the compliant panel derived from integrating the accelerometer data. When using the DIC data to obtain operational mode shapes, the DIC reference point is subtracted from the compliant panel DIC data to remove rigid body (tunnel) movement. However, it is instructive from a tunnel-noise perspective to look at the separate and disparate signals. The noise floor in the DIC measurements is readily apparent in the reference point measurement requiring the use of the accelerometer at the higher frequencies. A current challenge for the processing of the data is to distinguish contributions from the flow and panel movement from those of the tunnel at the lower frequencies. Naguib *et al*. presented an effective strategy for removing coherent content from time domain pressure signals using an optimal Wiener filter[27]. This, along with the methods proposed by Beresh *et al.*[28,29] are being investigated.

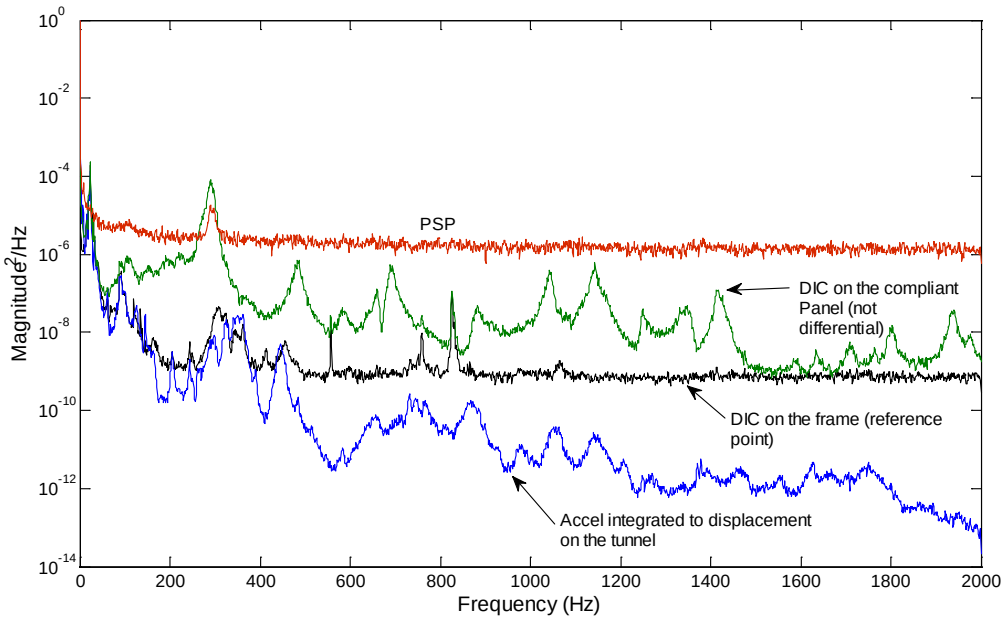

Figure 9: Tunnel low-frequency characteristics with accompanying panel center pressure (PSP) and displacement.

The use of PSP as a method to obtain the full field dynamic pressure provides unique insight for the interaction of a turbulent boundary layer with a compliant structure. However, it is not without its own set of challenges and issues. Recently Beresh *et al.* provided some useful insights into the measurement and data reduction for the condition of a turbulent boundary layer on a tunnel sidewall at Mach 3.0.[28,29] As they pointed out, an important feature in the measurement process of the turbulent boundary layer is the spatial size of the measurement area, the convection velocity near the wall, and the sampling frequency of the sensor. For the low-frequency measurements taken herein, the interaction of the spatial sensor size and the sampling frequency do not interact in a way to establish the cut off frequency of the measurement. However, each pixel in the image can be considered a square transducer with a measurement area of 0.077 mm^2, much smaller than the measurement area of a traditional Kulite sensor. In order to gain some insight into the effect of increasing the measurement size, a series of increasingly sized square-areas were averaged from the PSP data, monitoring the corresponding frequency content of the respective measurement. A different shock generator position, resulting in the shock impingement near the panel mid-point, was selected for this analysis. Unlike the flow condition/shock generator position of Figure 5, the present case provided a significant amount of area both up- and down-stream of the shock impingement region. Starting with an un-averaged PSP image as shown in Figure 10, four spatial locations were selected. Note that the numbers on the X- and Y-axes correspond to discrete pixels in the image. The first location is at the leading edge of the panel with respect to the flow direction. The second location was chosen just prior to the shock while the third was chosen in the middle of the shock. The final location was chosen farthest downstream. All points were in the centerline of the panel. In generating the spectral content of each point/area (PSD's), 14.5 seconds of data at the sampling rate of 4,000 Hz was used. The data was windowed using a Hanning function and a block size of 4096 sample points with averaging taking place using 50% overlap. This resulted in the PSD of the PSP data being averaged temporally 27 times. For comparison, Figure 11 shows the customary results from PSP where a 9 by 9 pixel moving average is used to smooth the data, and it should be noted that the data was in this form for the DMD analysis.

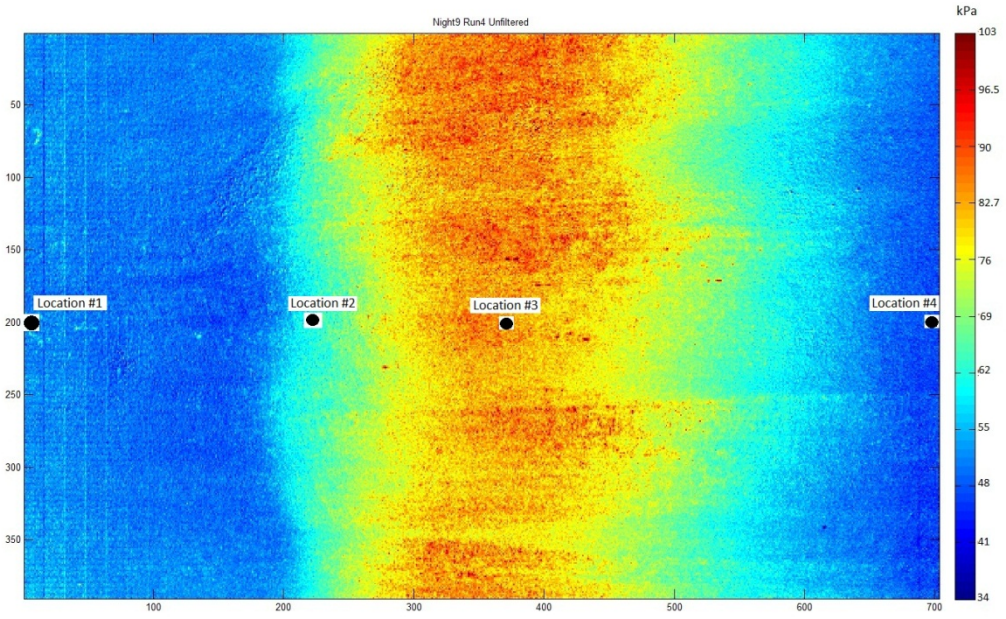

Figure 10: Shock at panel mid-point with no spatial averaging.

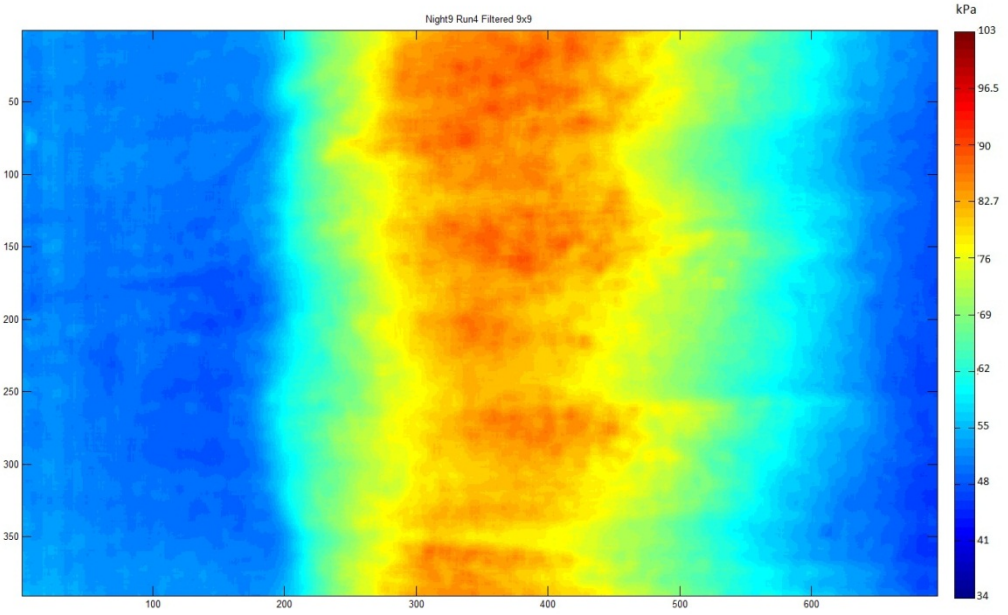

Figure 11: Shock at panel mid-point after applying a spatial 9x9 pixel moving average.

Figure 12-15 display the time history and frequency content for the four locations of Figure 11. As expected, an increase in measurement area resulted in less peak-to-peak variation. This is observed in the time history results, with little difference seen between the 7 by 7 and 11 by 11 pixel areas. The corresponding measurement size of a 3 by 3 pixel area is 0.833 mm square (0.7 mm^2), the 7 by 7 is 1.94 mm square (3.8 mm^2), and the 11 by 11 is 3.05 mm square (9.3 mm^2). In Figure 12, the location at the leading edge displays some interesting behavior. The panel movement should be small and hence the velocity of the plate should be small. However, the frequency content of the pressure corresponds directly to the dynamic content of the panel response. As the location is changed to

position 3, this behavior is overwhelmed by the strength of the shock. At location 4, down-stream of the shock front, a low frequency beating phenomena shows up in the 3 by 3 average (see the time history) yet is averaged out in the larger spatial averages. Additionally, the static pressure observed in the 11 by 11 average is greater than the 7 by 7 average easily seen in the time domain. This increase in static pressure was uncharacteristic of all other observations made to this point in this study. So in addition to removing unwanted measurement noise, selecting an optimal PSP "sensor size" is an ongoing area of study.

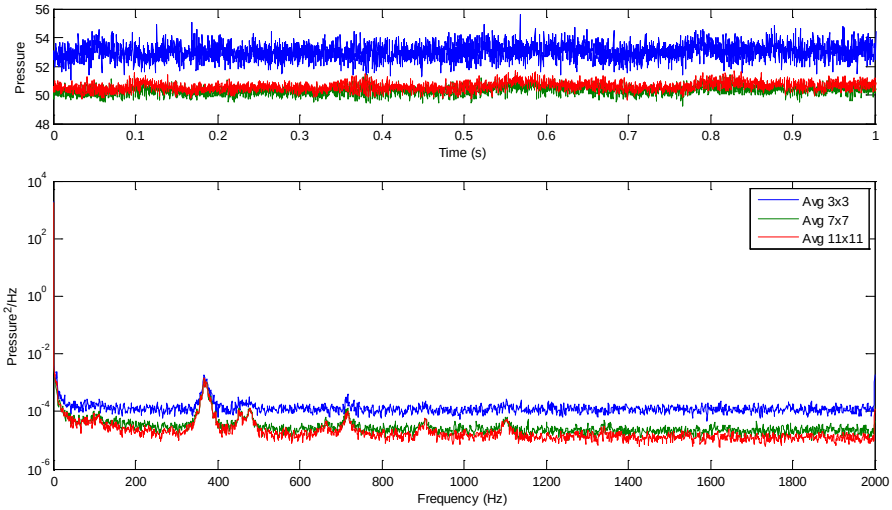

Figure 12: Time history and spectra for different spatial averages at Figure 10, location 1.

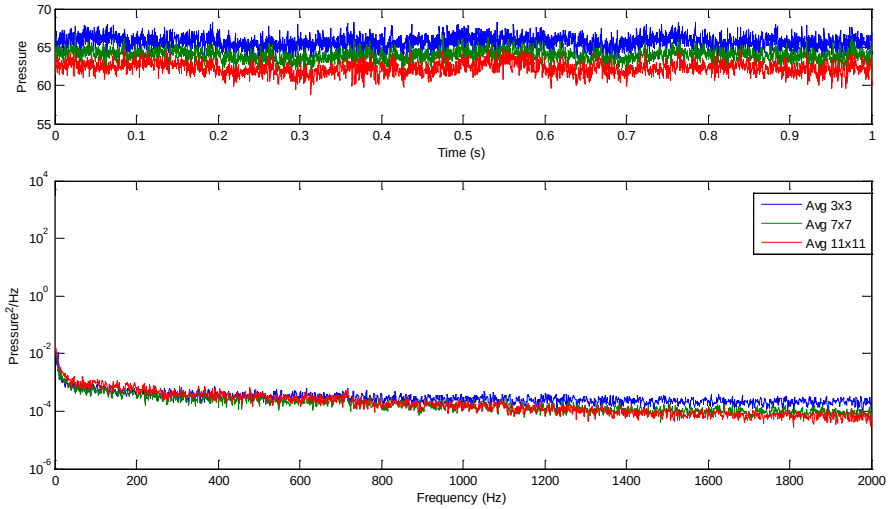

Figure 13: Time history and spectra for different spatial averages at Figure 10, location 2.

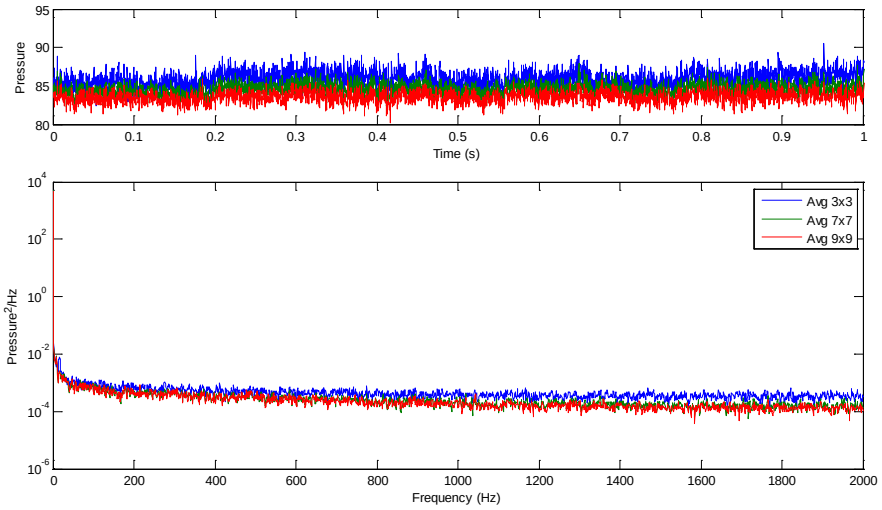

Figure 14: Time history and spectra for different spatial averages at Figure 10, location 3.

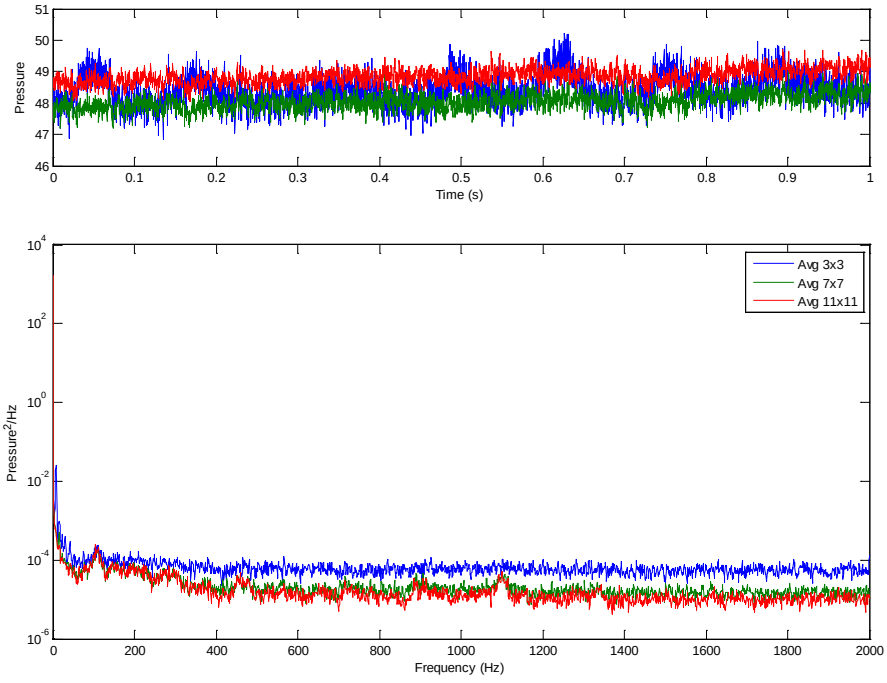

Figure 15: Time history and spectra for different spatial averages at Figure 10, location 4.

IV. Future Work

The U.S. Air Force is interested in testing and fielding hypersonic vehicles, and yet significant research needs to be done to better understand this harsh environment and those environmental interactions with the vehicle. The present experimental investigation was initiated to study the impact of a turbulent boundary layer, and a shock impingement, on the dynamic response of an aircraft-like dynamic panel. Several new experimental techniques were used to measure both the full-field input (surface pressure) and response (displacement) using novel optical techniques (DIC and PSP). These full-field techniques afforded the authors the ability to study the coherent structures in both

instances: operational modal analysis, proper orthogonal decomposition, and dynamic mode decomposition. It was also noted that the PSP surface pressure data requires averaging to quell spurious noise. Future work is planned to implement a more robust form of the dynamic mode decomposition by filtering the pressure snapshots via both a spatial average as well as using singular value decomposition to remove experimental "contamination". In this way, the snapshot data is projected onto a truncated set of proper orthogonal modes. These more robust pre-processing steps, along with the use of adaptive time-domain filters, will be effective in mitigating experimental noise. Once a sufficient and compact set of surface pressure modes are identified, this basis can be used as inputs to a nonlinear structural reduced order model.[26] It would be desirable to couple the reduced-order structural model to a corresponding aerodynamic surrogate model and study the effects of the various flow conditions offered in the RC-19 facility.

Acknowledgments

The authors gratefully acknowledge the support of Dr. David Stargel of the Air Force Office of Scientific Research (AFOSR), LRIR number 12RB04COR.

References

[1] R. Quiroz, J. Embler, R. Jacobs, G. Tzong, and S. Liguore, "Predictive Capability for Hypersonic Structural Response and Life Prediction: Phase II – Detailed Design of Hypersonic Cruise Vehicle Hot-Structure ," Technical Report, AFRL-RQ-WP-TR-2012-0265, February 2012.

[2] B. Zuchowski, "Predictive Capability for Hypersonic Structural Response and Life Prediction: Phase II – Detailed Design of Hypersonic Cruise Vehicle Hot-Structure," Technical Report, AFRL-RB-WP-TR-2012-0280, May 2012.

[3] J.D. Leatherwood, S.A. Clevenson, C.A. Powell, E.F. Daniels, "Acoustic Testing of High-Temperature Panels," Journal of Aircraft, Vol. 29 (1992), pp. 1130 - 1136.

[4] B.M. Miller, J.J. McNamara, S.M. Spottswood, A.J. Culler, "The Impact of Flow Induced Loads on Snap-Through Behavior of Acoustically Excited, Thermally Buckled Panels," Journal of Sound and Vibration, Vol. 330, pg. 5736-5752, 2011.

[5] R.D. Blevins, I. Holehouse, "Thermoacoustic Loads and Fatigue of Hypersonic Vehicle Skin Panels," Journal of Aircraft, Vol. 30 (1993) pp. 971-978.

[6] L. Maestrello, T.L.J. Linden, "Measurements of the response of a panel excited by shock boundary-layer interaction," Journal of Sound and Vibration (1971) 16 (3), 385-391.

[7] C.F. Coe, W.J. Chyu, "Pressure-Fluctuation Inputs and Response of Panels Underlying Attached and Separated Supersonic Turbulent Boundary Layers," NASA TM X-62,189, September 1972.

[8] P. Pozefsky, "Identifying Sonic Fatigue Prone Structures on a Hypersonic Transatmospheric Vehicle," AIAA 12th Aeroacoustics Conference, April 10-12, 1989, San Antonio, Texas.

[9] D.S. Dolling, "Unsteadiness of Shock-Induced Turbulent Separated Flows – Some Key Questions," 31st AIAA Fluid Dynamics Conference & Exhibit, 11-14 June 2001, Anaheim, California.

[10] D.S. Dolling, "Fifty Years of Shock-Wave/Boundary-Layer Interaction Research: What Next?" AIAA Journal, Vol. 39, No. 8, August 2001.

[11] T. Beberniss, S. Spottswood, T. Eason, "High-Speed Digital Image Correlation Measurements of Random Nonlinear Dynamic Response," SEM Annual Conference, Uncasville, CT, June 10-13, 2011.

[12] T. Beberniss, T. Eason, S. Spottswood, “High-speed 3D digital image correlation measurements of long-duration random vibration; recent advancements and noted limitations,” Proceedings, International Conference on Noise and Vibration Engineering (ISMA), KatholiekeUniversiteit Leuven, Belgium, 2012.

[13] S. Spottswood, T. Eason, T. Beberniss, “Influence of Shock-Boundary Layer Interactions on the Dynamic Response of a Flexible Panel,” Proceedings, International Conference on Noise and Vibration Engineering (ISMA), KatholiekeUniversiteit Leuven, Belgium, 2012.

[14] M.R. Gruber, A.S. Nejad, “Development of a Large-Scale Supersonic Combustion Research Facility,” 32nd AIAA Aerospace Sciences Meeting & Exhibit, January 10-13, 1994, Reno, Nevada, AIAA Paper 94-0544.

[15] M. Sutton, J. Orteu, Schreier, H, "Image Correlation for Shape, Motion, and Deformation Measurements: Basic Concepts, Theory and Application", Springer Science+Business Media, LLC, ISBM#: 978-0-387-78746-6, 2009.

[16] J. Crafton, A. Forlines, S. Palluconi, K.Y. Hsu, C. Carter, M. Gruber, “Investigation of Transverse Jet Injections in a Supersonic Crossflow Using Fast Responding Pressure-Sensitive Paint,” 29th AIAA Applied Aerodynamics Conference, 27-30 June 2011, Honolulu, Hawaii.

[17] W. Flaherty, J. Crafton, G.S. Elliot, and J.M. Austin, “Application of fast pressure sensitive paint in hypervelocity flow,” 49th AIAA Aerospace Sciences Meeting, 4-7 January 2011, Orlando, Florida.

[18] ARAMIS, v.6.1.1 User's Manual, Revision C, GOM mdH, Braunschweig, Germany, 2009.

[19] S. Chauhan, R. Martell, R.J. Allemang, D.L. Brown, "Implementation of complex frequency mapping to low order frequency domain algorithm for operational modal analysis," Proceedings of the International Modal Analysis Conference, Springfield, Massachusetts, 2007.

[20] R. Brincker, L. Zhang, P. Andersen, "Modal identification of output-only systems using frequency domain decomposition," Smart Materials and Structures (2001), 10, 441-445.

[21] R.J. Allemang, D.L. Brown, "A complete review of the complex mode indicator function (CMIF) with applications," Proceedings of the ISMA International Conference on Noise and Vibration Engineering, KatholiekeUniversiteit, Leuven, Belgium, 2006.

[22] C.W. Rowley, I. Mezic, S.Bagheri, P.Schlatter, D.S. Henningson, “Spectral analysis of nonlinear flows,” Journal of Fluid Mechanics (2009), 641, 115-127.

[23] P.J. Schmid, K.E. Meyer, O. Pust, “Dynamic Mode Decomposition and Proper Orthogonal Decomposition of flow in a lid-driven cylindrical cavity,” 8th International Symposium on Particle Image Velocimetry – PIV09, Melbourne, Victoria, Australia, August 25-28, 2009.

[24] P.J. Schmid, “Dynamic mode decomposition of numerical and experimental data,” Journal of Fluid Mechanics (2010), 656, 5-28.

[25] P.J. Schmid, “Application of the dynamic mode decomposition to experimental data,” Experimental Fluids (2011), 50, 1123-1130.

[26] M.P. Mignolet, A. Przekop, S.A. Rizzi, S.M. Spottswood, "A review of indirect/non-intrusive reduced order modeling of nonlinear geometric structures," Journal of Sound of Vibration (2013), 332, 2437-2460.

[27] A.M. Naguib, S.P. Gravante, C.E. Wark, “Extraction of turbulent wall-pressure time-series using an optimal filtering scheme,” Experiments in Fluids (1996) 22, 14-22.

[28] S.J. Beresh, J.F. Henfling, R.W. Spillers, B.O. Pruett, “Measurement of fluctuating wall pressures beneath a supersonic turbulent boundary layer,” 48th AIAA Aerospace Sciences Meeting, Orlando, FL, AIAA 2010-305.

[29] S.J. Beresh, J.F. Henfling, R.W. Spillers, B.O. Pruett, "Pressure power spectra beneath a supersonic turbulent boundary layer", 48th Fluid Dynamics Conference and Exhibit, Chicago, IL, AIAA 2010-4274.